

Origin of Coulomb blockade oscillations in single-electron transistors fabricated with granulated Cr/Cr₂O₃ resistive microstrips

Xiangning Luo*, Alexei O. Orlov, Gregory L. Snider

Department of Electrical Engineering, University of Notre Dame, Notre Dame, IN 46556, USA

Available online 23 March 2005

Abstract

The purpose of our work is to evaluate single-electron devices fabricated using resistive microstrips and to investigate its applicability for single-electron logic. In this article, we present our work on the fabrication and characterization of SETs with gold islands and CrO_x resistive microstrips. The electron transport mechanism of CrO_x resistors is also discussed and hypothesis of two types of possible junctions are given as the explanation for the experimental results.

© 2005 Elsevier Ltd. All rights reserved.

Keywords: Single-electron transistor; Coulomb blockade; Tunnel junctions

1. Introduction

The single electron tunneling transistor (SET) [1,2] is a device based on Coulomb blockade of tunneling. Typical metal-film SET consists of a small (micron size) metal island connected to the external circuits with two tunnel junctions and a gate capacitively coupled to the island. For an SET to operate, the total capacitance of the island, C , must be small enough that the charging energy $E_C = e^2/2C$ is much greater than the thermal energy, $k_B T$. The second condition imposed by the uncertainty principle is that the resistance of the tunnel barriers, R_T must exceed the resistance quantum $R_Q = h/2e^2 \approx 13 \text{ k}\Omega$. If these conditions are satisfied, the number of electrons on the island is fixed, and extra energy is needed to add an extra electron to the island (Coulomb blockade of tunneling). The blockade conditions could be lifted by changing the gate bias. If a small bias is applied between the junction which form source and drain of a SET, the tunneling current through the SET changes periodically as a function of applied gate voltage with a period of $V_g = e/C_g$, where C_g is a capacitance between the island and a gate. The quantization of energy levels in the island could be neglected for metallic islands with the size greater than some 100 nm even at miliKelvin

temperatures and the system could be completely described by an orthodox theory of Coulomb blockade [3].

Since the first implementation of the SET where tunneling barriers made of Al₂O₃ were sandwiched between thin layers of Al island using Dolan-bridge technique [1], a number of different geometries, materials and methods have been used for the fabrication of thin metal film single electron transistors [3–5]. Despite some differences all these devices share the same basic design—a metal island isolated by two tunnel junctions. Recently, a general theory of Coulomb blockade was proposed by Nazarov [6]. According to this theory, tunnel junctions are not necessary to provide insulation required for discrete charging effects and they may be replaced by arbitrary scatterers, including tunnel junctions, quantum point contacts, and diffusive conductors. The scatterer of the same resistance as a tunnel junction suppresses Coulomb blockade exponentially by a factor of $\exp(-\alpha G/G_Q)$, where α is a dimensionless parameter depending on the type of the conductor, and $G_Q = 1/R_Q$. It is important to note, that the requirement on the capacitance, $C \ll e^2/2k_B T$, for the scatterers discussed in Ref. [6] is fulfilled by assumption.

Combination of junctions and resistors was studied in Ref. [7] where SETs were made with Cr resistive microstrips augmenting tunnel junctions, Nb SETs with ‘weak links’ made by combined shadow evaporation and anodization [8], and more recently single-electron transistors with metallic microstrips instead of tunnel junctions were reported [9]. One important advantage of the devices

* Corresponding author. Tel.: +1 574 6316707.
E-mail address: xluo@nd.edu (X. Luo).

combining resistors and junctions is a strong suppression of co-tunneling (a second order coherent quantum process consisting of multiple simultaneous tunneling events). The experiments by Lotkhov et al. [7] showed that microstrips with resistance nR_Q act as n tunnel junctions connected in series, strongly suppressing the cotunneling. In quantum-dot cellular automata (QCA) [10,11] devices, cotunneling severely impairs the ability of cells to store information. To suppress cotunneling, complicated multiple-tunnel junction (MTJ) structures were used in Ref. [12]. By replacing MTJ with resistive microstrips, the number of junctions can be reduced. This eliminates the problem of junction random background charge compensation in extra dots of MTJs and greatly simplifies the design of cells.

2. Fabrication

The single-electron transistors, comprising the Au electrodes, island and CrO_x microstrips (see Fig. 1) were fabricated using two steps of e-beam lithography and metal deposition. In the purpose of eliminating the problem of parasitic junction formation caused by native Al oxide, Au is chosen instead of Al as the island metal. Two versions of SET island wiring geometry (WG), with one continuous CrO_x wire atop a gold island, WG1 (Fig. 1a), and two CrO_x

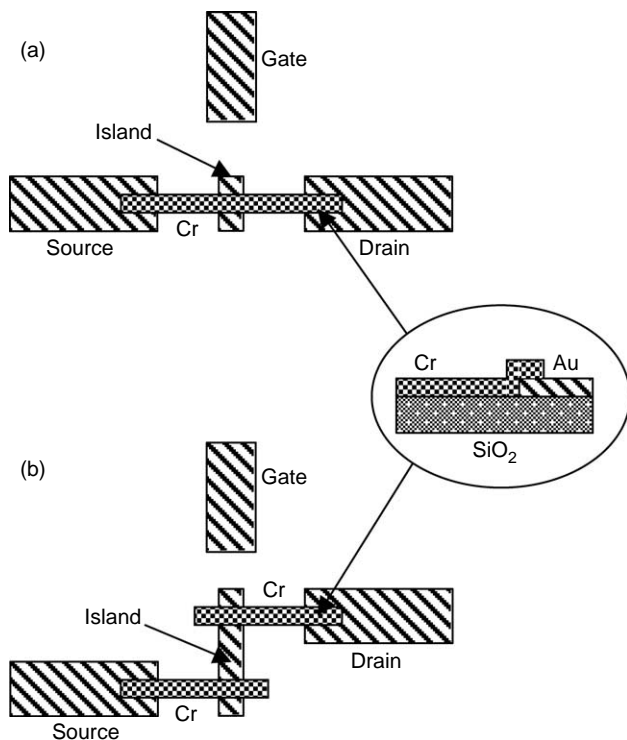


Fig. 1. Two versions of SET wire geometry, (a) with one continuous CrO_x wire atop a gold island; (b) with two CrO_x wires connecting a gold island to source and drain. The inset is the cross-section at the overlap area of Au layer and CrO_x layer. The CrO_x wires are 0.375–2 μm long, 70 nm wide, and 6–10 nm thick. The thickness of Au layer is 10 nm. The size of Au island is varied from 200 nm by 500 nm to 300 nm by 1 μm .

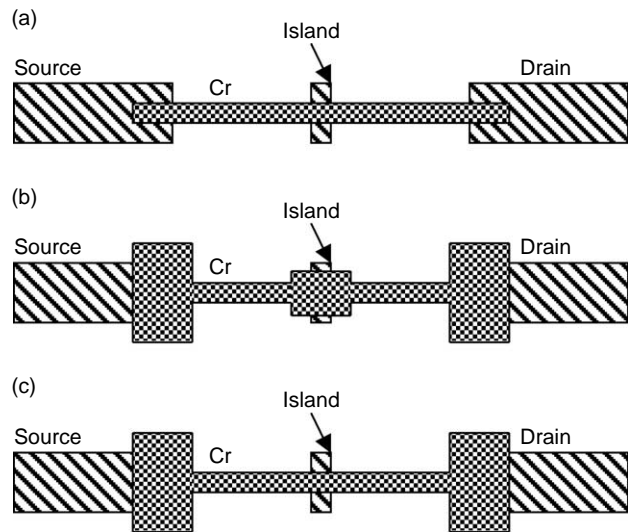


Fig. 2. Schematic view of three types of pattern design. (a) Type #1: CrO_x layer consists of narrow lines (~ 70 nm) only. (b) Type #2: large tabs (wider than 300 nm in two dimensions) on both ends cover all of the steps where the two layers of metal overlap. (c) Type #3: large tabs only cover the steps of source and drain and no tabs appear on the island.

wires connecting a gold island to source and drain, WG2 (Fig. 1b) are used in all of our experiments. Each version of geometry has three types of microstrip Contact Pattern Design (CPD) which will be expanded below. No significant difference between WG1 and WG2 was observed in the electrical characterizations. For simplicity, Fig. 2 shows only the three types of CPD using wire design WD1. First layer e-beam lithography and metal deposition define the Au electrodes and island (2 nm Ti and 10 nm Au). The CrO_x resistive microstrips connecting the island to the electrodes are formed in the second e-beam lithography and deposition step. In the second metal deposition, a thin film of Cr was evaporated in the oxygen ambient. By controlling the oxygen pressure and deposition rate, different values of sheet resistance of CrO_x film were achieved. Each type of pattern was used in the devices with 8–10 nm thick CrO_x and thicker layer (~ 40 nm) of CrO_x devices were tested using the third pattern.

3. Characterization of CrO_x resistors

To obtain high quality CrO_x resistive microstrips with controllable resistivity, we performed extensive characterization of the deposition process. In situ measurements were taken to monitor the resistance of the microstrips during deposition of Cr in an O_2 ambient at different oxygen pressures. The results showed that the wires became conducting when the film thickness reached ~ 2 nm. For 10 nm thick CrO_x , sheet resistances in the range of 1–10 $\text{k}\Omega/\square$ were formed when the oxygen pressure was around 3.6×10^{-5} Torr in our evaporation system with a deposition rate of 0.05 nm/s. A slightly higher

(-4.5×10^{-5} Torr) oxygen pressure resulted in much higher sheet resistance and the films were completely insulating with even higher pressure.

Chromium has three common oxides [13]. Cr_2O_3 is an insulator with stable chemical prosperities and has a green color, CrO_3 is an n-type semiconductor with a dark red color, and CrO_2 is a half-metal ferromagnet [14] with a black color. When the temperature is higher than 250°C , CrO_3 and CrO_2 decompose into Cr_2O_3 and O_2 . In our experiments, the color of sample holder was always green after deposition of CrO_x film with sheet resistance of $\leq 5 \text{ k}\Omega/\square$ and the resistance of the CrO_x was always infinity when red color was observed. Similar results were obtained by other groups for similar deposition process [9].

To study the transport mechanism of the CrO_x microstrips, we characterized strips with the same dimensions to those used in the single-electron transistor samples. We believe that the resistive microstrips consist of granules where each granule consists of a Cr core with a Cr_2O_3 shell. Electrons are tunneling from granule to granule through the Cr_2O_3 insulating layer, and higher oxygen content gives a thicker shell that changes the conductance behavior from metallic to insulating as intergranular oxide resistance approaches R_0 . I - V characteristic of the microstrips in this case is strongly nonlinear due to intergranular Coulomb blockage [15]. For microstrips with sheet resistance $R \leq 3 \text{ k}\Omega/\square$, weak temperature dependence, almost linear four, and no Coulomb blockade oscillations are observed down to 0.3 K .

4. Characterization of single-electron transistors with thin CrO_x wires

To form SETs, and study the origin of the Coulomb blockade in our devices, three types of patterns (Fig. 2) in each of the two versions of Fig. 1 were fabricated with 8 – 10 nm thick CrO_x . In all of these, the first layer of metal (Au) is the same, defining the islands and electrodes. The difference is only in the second layer (CrO_x) at the overlap areas.

In the first type of CPD design (type #1, Fig. 2a), the CrO_x layer consists of narrow lines ($\sim 70 \text{ nm}$) without tabs on the overlap areas. Very small number ($< 20\%$) of devices showed finite conductance at room temperature with broad distribution of the resistance values. Most of the devices degraded rapidly to an open circuit when exposed to air. Therefore, no low temperature data were obtained for these devices. A possible source of these failures is a step-coverage problem.

In the second type of CPD (type #2, Fig. 2b), the large tabs (wider than 300 nm in two dimensions) on both ends of the lines cover all of the steps where the two layers of metal overlap. Over 95% devices showed conductance at room temperature. The CrO_x films were rather uniform (variation $\pm 20\%$) and lasted for a relatively long time when exposed

Table 1
Yield vs. resistance

Resistance range	$R < 100 \text{ k}\Omega$	$100 < R < 200 \text{ k}\Omega$	$200 \text{ k}\Omega < R < 1 \text{ M}\Omega$	$R > 1 \text{ M}\Omega$
Total number of devices	12	9	5	4
Number of devices showed CBO	0	5	3	3
Yield (%)	0	56	60	75

to air. In the range of 2 – $7 \text{ k}\Omega/\square$, significant nonlinearities around zero bias and strong temperature dependence characteristic of hopping conductance are observed (in the devices with sheet resistance greater than $7 \text{ k}\Omega/\square$, conductance was ‘freezing out’ below 5 K); however, none of the devices exhibited Coulomb blockade oscillations. These experimental results indicate that resistive microstrip itself does not provide Coulomb blockade of electrons on the island.

In the third type of CPD (type #3, Fig. 2c), large tabs cover only the steps of source and drain and no tabs appear on the island. The room temperature measurements showed that 95% devices were conducting, with good uniformity of resistance. However, among those devices having significant nonlinearity in I - V curves at 300 mK , only about 30% exhibited Coulomb blockade oscillations. From a study of the yield vs. resistance (Table 1), we found that Coulomb blockade oscillations were only observed when the resistance of devices was greater than $100 \text{ k}\Omega$ at 0.3 K , and devices with higher resistance were more likely to show Coulomb blockade oscillations. The value of charging energy was varying significantly for the devices of the same batch (0.01 – 1 meV). The two devices which have the largest charging energy ($\sim 0.4 \text{ meV}$) had about $5 \text{ M}\Omega$ resistances at the ‘open’ state (when the Coulomb blockade is lifted) at 300 mK . The I - V curve (Fig. 3a) and I - V_g modulation curve (Fig. 3b) of one of the devices clearly demonstrate single-electron transistor behavior with strong nonlinearity in the open state.

5. Characterization of single-electron transistors with thicker CrO_x wires

SETs with thicker ($\sim 40 \text{ nm}$) CrO_x wires were also fabricated using CPD type #3 (Fig. 2c) with different widths of the island (80 and 500 nm). The room temperature sheet resistance of the devices showing significant nonlinearity in I - V curves at 300 mK is around $5 \text{ k}\Omega/\square$, which is about the same as our previous SETs with thinner (8 – 10 nm) CrO_x wires. However, among those devices having significant nonlinearity, about 95% (21 out of 22) exhibited Coulomb blockade oscillations (Fig. 4a), which is much higher than that of SETs with thinner CrO_x wires. The charging diagram of one of the SETs is presented in Fig. 4b.

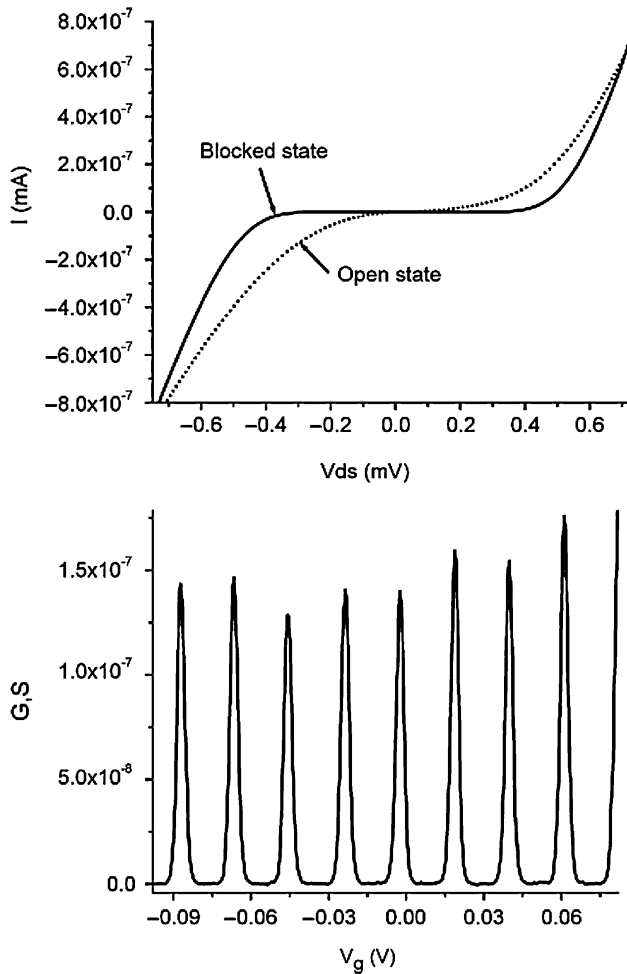


Fig. 3. (a) I - V curves of an SET in open state and blocked state. (b) I - V_g modulation curve of the same SET of (a) measured at 300 mK showed deep modulation by the gate. Charging energy is about 0.4 meV.

These characteristics clearly demonstrate the typical SET behavior. For the 80 nm wide Au island devices, the period of Coulomb blockade oscillations is 16 mV and it is 6 mV for the devices with 500 nm wide Au island, which are consistent with the calculation using FASTCAP.

6. Discussion

Based on these observations, we conclude that in the devices with 8–10 nm thick CrO_x microstrips which show Coulomb blockade oscillations some sort of weak links with small intrinsic capacitance and $R > R_Q$ are formed at the edges of the CrO_x wires overlapping the Au islands. Indeed, the Coulomb blockade is observed only on those samples with narrow lines (~ 70 nm) overlapping the island (type #3) (Fig. 5). The CrO_x line must be thinner at the overlapping edges where it climbs onto the island. Taking into account the thickness of the island metal (12 nm) and the thickness of the CrO_x strips (8–10 nm) it is likely that the CrO_x at these edges has breaks or is more readily oxidized

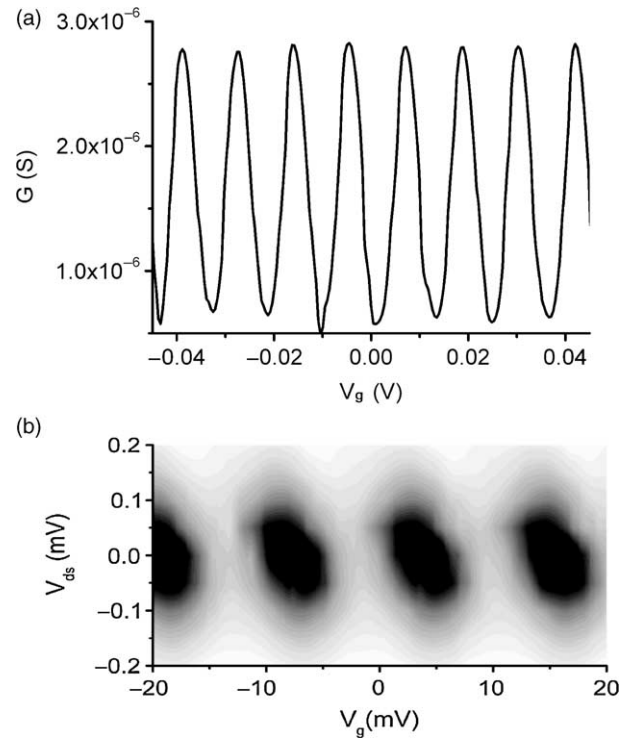


Fig. 4. (a) I - V_g modulation curves of an SET with 40 nm thick CrO_x strips showed deep modulation by the gate. (b) Charging diagram of the same SET of (a) measured at 12 mK.

than along the strip, forming weak links to the island. The number of oxidized granules in the 70 nm wide line is about 10–20 (grain size 5–15 nm [16]). These weak links, which consist of a few oxidized Cr granules, having small capacitance with resistance $\geq R_Q$ comprise the low-capacitance junctions needed for Coulomb blockade of electrons on the island. Large size of grains in Au film might contribute to a weak link formation. The single period of I - V_g modulation curves indicates, however, that there are only two junctions (one island) in those devices. In devices with the large tabs covering the steps it is likely that shorting

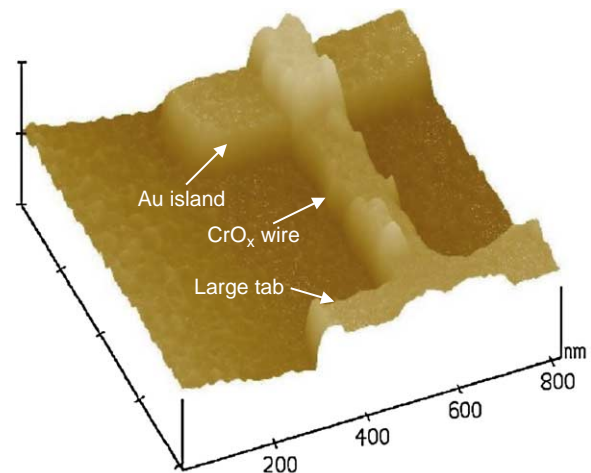


Fig. 5. AFM image of a CrO_x wire deposited on the edge of Au island.

bridges are formed across the steps and/or that the capacitance was sufficiently large to suppress Coulomb blockade effects at a temperature of 0.3 K. The charging energy ($E_C = e^2/2C$) depends on the total capacitance of the island which is dominated by the capacitances of the tunnel junctions. Large variation in oxide thickness of weak link junctions leads to large variation in junction capacitance. Thus, the value of charging energy varied significantly for the devices of the same batch. Exposure to air after fabrication leads to further oxidation of the devices. Oxidation of the CrO_x granules at the weak links causes the observed degradation of devices. Type 1 devices have two more weak links than type 3, and one weak link's failure degrades the whole device. Thus, Type 1 devices should degrade faster than type 3 devices. In addition, type 1 devices have higher resistivity than the other two types of devices and our experiments showed that devices with higher resistivity degraded faster. We also fabricated wires with width 1–100 μm with all of which showed a small variation ($\sim 10\%$) in the resistance over time (several weeks).

For those devices with thicker CrO_x strips, we believe that tunnel junction formation is slightly different than in the devices with thinner CrO_x wires. Since in these devices CrO_x layer is much thicker than the Au island, step coverage could be ruled out as a cause for junction formation. To get the same sheet resistance, the bulk resistivity need to be about 4 times larger for thicker CrO_x wires, which means the Cr granules in the thicker CrO_x wire have thicker Cr_2O_3 shell. The Cr_2O_3 shells right above the Au island can act as tunnel barriers providing small enough capacitance and resistance larger than R_Q to fulfilled the two requirements of Coulomb blockade oscillations.

An undesirable property of the above fabrication methods, is that the junctions are formed randomly. A significant number of devices did not show SET behaviors even though they had the same pattern design and sheet resistance as those that showed oscillations. More experiments, including TEM inspection, are needed, however, to confirm the origin of the junctions in this kind of devices.

7. Summary

We present experimental investigation of the origin of Coulomb blockade in the SETs with resistive microstrips with no intentional tunnel junctions, fabricated using technology similar to [3]. By using Au instead of Al for SET island material we eliminate a possibility of unintentional oxidation of the island in the fabrication process. By varying the area and the thickness of the microstrip regions overlapping the Au island we show that the Coulomb blockade which leads to SET operation is not caused by

the presence of microstrips but roots from randomly formed weak links at the edges of the Au island. The formation of such weak links is naturally more likely for more resistive strips. Once the step coverage becomes uniform and weak links are eliminated, Coulomb blockade of electrons on Au island becomes strongly suppressed as equivalent capacitance of such 'junction' becomes large. Our experiments show that the formation of tunneling barriers capable to fulfill the two requirements of Coulomb blockade remains crucial for the observation of Coulomb blockade phenomenon.

Acknowledgements

We are very thankful to A. Korotkov (UC Riverside) for performing FASTCAP calculations and attention to this work. The authors wish to thank V.A. Krupenin, B.I. Shklovskii for multiple useful discussions. R. Kumamuru and K. Yadavalli's assistance in the measurements is gratefully acknowledged. This work was supported by the MRSEC Center for Nanoscopic Materials Design of the National Science Foundation under Award Number DMR-0080016.

References

- [1] T.A. Fulton, G.D. Dolan, *Physical Review Letters* 59 (1987) 109.
- [2] K.K. Likharev, *IEEE Transactions on Magnetics* 23 (1987) 1142.
- [3] K.K. Likharev, *Proceedings of the IEEE* 87 (1999) 606.
- [4] A. Notargiacomo, L. Di Gaspare, G. Scappucci, G. Mariottini, E. Giovine, R. Leoni, F. Evangelisti, *Materials Science and Engineering C* 23 (2003) 671.
- [5] K. Matsumoto, S. Kinoshita, Y. Gotoh, K. Kurachi, T. Kamimura, M. Maeda, K. Sakamoto, M. Kuwahara, N. Atoda, Y. Awano, *Japanese Journal of Applied Physics* 42 (2003) 2415 (Part 1: regular papers and short notes and review papers).
- [6] Y.V. Nazarov, *Physical Review Letters* 82 (1999) 1245.
- [7] S.V. Lotkhov, S.A. Bogoslovsky, A.B. Zorin, J. Niemeyer, *Applied Physics Letters* 78 (2001) 946.
- [8] T. Henning, D.B. Haviland, P. Delsing, *Superconductor Science and Technology* 10 (1997) 727–732.
- [9] V.A. Krupenin, A.B. Zorin, M.N. Savvateev, D.E. Presnov, J. Niemeyer, *Journal of Applied Physics* 90 (2001) 2411.
- [10] P.D. Tougaw, C.S. Lent, *Journal of Applied Physics* 75 (1994) 1818.
- [11] C.S. Lent, P.D. Tougaw, W. Porod, G.H. Bernstein, *Nanotechnology* 4 (1993) 49.
- [12] A.O. Orlov, R.K. Kumamuru, R. Ramasubramaniam, G. Toth, C.S. Lent, G.H. Bernstein, G.L. Snider, *Applied Physics Letters* 78 (2001) 1625.
- [13] S. Budavari, *The Merck Index, An Encyclopedia of Chemicals, Drugs, and Biologicals*, Merck, Rahway, NJ, 1989.
- [14] K. Schwarz, *Journal of Physics F: Metal Physics* 16 (1986) L211.
- [15] B.I. Shklovskii, *Fiz. Tekh. Poluprovodn* 10 (1976) 1440.
- [16] M. Ohring, *The Materials Science of Thin Films*, Academic Press, London, 1992.